Radiometric calibration of an ultra-compact microbolometer thermal imaging module

David W. Riesland[a], Paul W. Nugent[a], Seth Laurie[a], and Joseph A. Shaw[a*]

[a]Montana State University, Electrical and Computer Engineering, 610 Cobleigh Hall, Bozeman, MT, 59717

ABSTRACT

As microbolometer focal plane array formats are steadily decreasing, new challenges arise in correcting for thermal drift in the calibration coefficients. As the thermal mass of the cameras decrease the focal plane becomes more sensitive to external thermal inputs. This paper shows results from a temperature compensation algorithm for characterizing and radiometrically calibrating a FLIR Lepton camera.

Keywords: optics, photonics, microbolometer, calibration, Lepton, temperature compensation

1. INTRODUCTION

Uncooled microbolometer focal plane array (FPA) technologies have been steadily decreasing in format over the past decade. The Optical Remote Sensor Lab (ORSL) at Montana State University has been characterizing uncooled microbolometers for environmental remote sensing applications since the early 2000s under Dr. Joseph A. Shaw. Different applications have included detection of bee hive health,[1] characterization of thermal pools in Yellowstone National Park,[2,3] detection of CO_2 leaks,[4] cloud characterization for climate studies,[5–8] cloud detection and classification for earth-space communications,[9–12] and measuring the moon and optical properties of smoke layers in the atmosphere.[13]

Further author information: (Send correspondence to Joseph A. Shaw)
Joseph A. Shaw: E-mail: joseph.shaw@montana.edu, Telephone: 1 406 994 7261

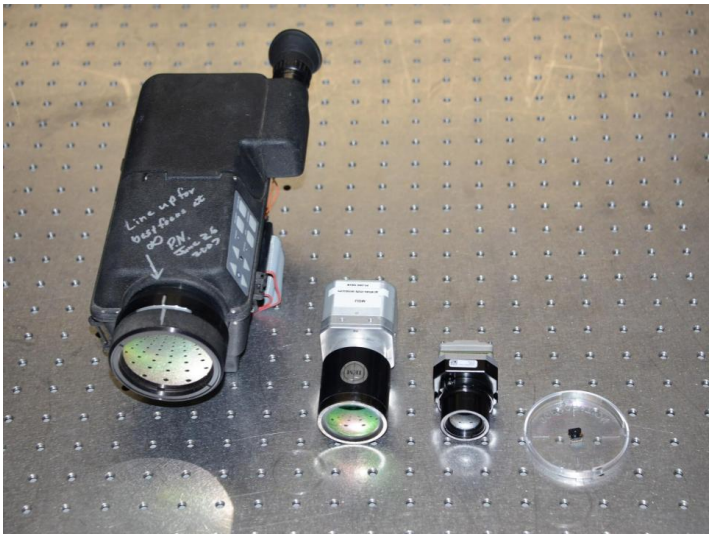

Figure 1: Uncooled microbolometer formats have decreased dramatically over time. FLIR cameras are shown from left to right: 1999 (Amber Sentinel), 2006 (FLIR Photon 320), 2013 (FLIR Tau2), and 2016 (FLIR Lepton).

Thermosense: Thermal Infrared Applications XXXIX, edited by Paolo Bison, Douglas Burleigh, Proc. of SPIE
Vol. 10214, 1021417 · © 2017 SPIE · CCC code: 0277-786X/17/$18 · doi: 10.1117/12.2262956

All of these applications require radiometric calibration of the camera, which is provided with methods we have developed for characterizing and compensating for the camera response as it changes with the focal-plane-array temperature.[14–16] Figure 1 shows four types of uncooled microbolometer cores calibrated over the past two decades at ORSL. As the size of these focal planes continue to decrease, internal mechanical mechanisms become more influential on FPA temperature. Because of this, new methods must be explored to compensate for the new influences of thermal drift on the smaller uncooled microbolometer cores.

2. FOCAL PLANE COMPENSATION AND CALIBRATION

Since the microbolometer FPA is inherently a resistive device, a change in ambient temperature leads to a resistance change that causes measurement drift. One of the ways to account for this drift is to model the expected temperature response of the FPA as a function of deviation from a nominal temperature, as discussed extensively in Ref. 14,15. This compensated response is then calibrated pixel-by-pixel into radiance values using a regression of collected blackbody data as FPA temperature is varied over normal operating conditions.

The calibration method involves running the camera under test in an environmental chamber while viewing a calibrated blackbody. The blackbody is held at 6 different temperatures while the environmental temperature is slowly swept through temperatures expected to be experienced by the camera during its normal operation. This method has been used at Montana State University (MSU) to calibrate both FLIR Photon and Tau2 cameras in the past with very good results. Photon FPA calibrations have been able to reproduce blackbody target radiance values with a standard deviation of 0.35 W/(m^2 sr).[8]

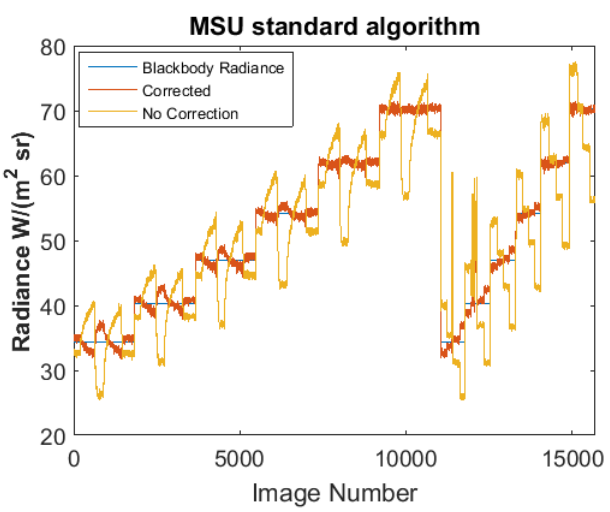

(a) Camera corrected radiance is shown for each image in the testing sample set.

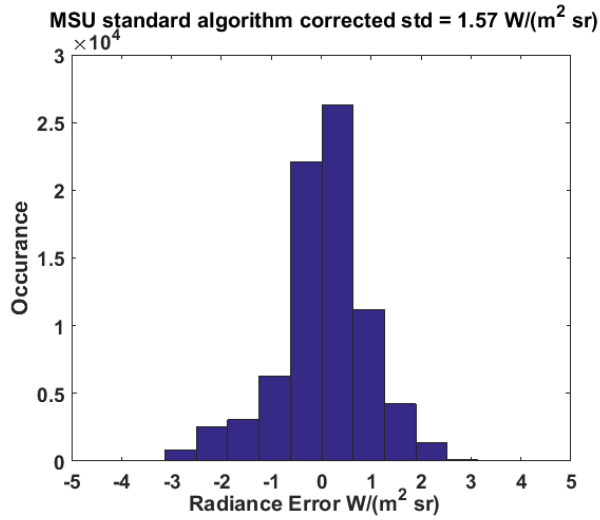

(b) Error distribution in radiance for MSU standard calibration algorithm.

Figure 2: Lepton calibration results via MSU standard method.

With this history of calibrating microbolometer cameras for quantitative remote sensing applications, it was natural to see how well we could calibrate the FLIR Lepton ultra-low-cost IR imaging module. The standard method developed at MSU for the Photon and Tau2 cameras allowed for a fairly good calibration of the Lepton camera. The reproducibility of the Lepton was about three times that of the standard deviation seen from the Photon FPA at 1.57 W/(m^2 sr). The calibrated image radiance is plotted vs the image number in Fig. 2a as the camera viewed a blackbody calibration source whose temperature was varied in a staircase pattern; the distribution of radiance errors can be seen in Fig. 2b.

Although the average corrected radiance over time appears to have low variability, the pixel-by-pixel gain used for the correction shows that there is high non-uniformity throughout the image. This can be seen clearly in Fig. 3. The ramifications of this effect have not been fully explored, but future applications should keep this in mind.

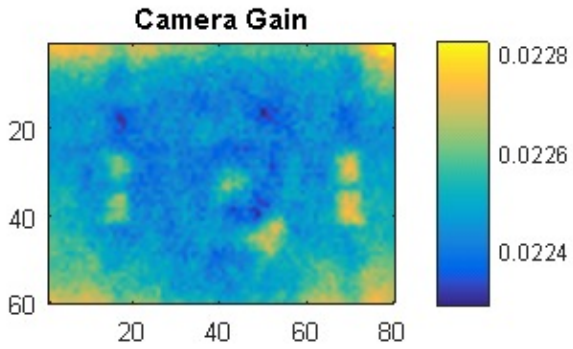

Figure 3: Camera correction for the focal plane shows non-uniform hot spots that appear to be circuit components.

3. DATA VALIDATION

In order to test the viability of the Lepton camera for environmental remote sensing, we took our assembled camera unit outside to look at various objects. The camera had better than expected sensitivity, being able to distinguish cloud spatial variability quite well (although with very low spatial resolution). Figure 4a shows the Lepton camera mounted to a Raspberry Pi board, which is then attached to a tripod. This assembly was pointed to the horizon overlooking the MSU campus. In Fig. 4b a person is seen waving to the camera, while a cloudy sky is shown overhead. Montana Hall, the building with the spire sticking up at the bottom right corner of Fig. 4a, also stands out from the background in Fig. 4b. For this image, the ambient temperature was about 0 °C. It is interesting to note that even with the fairly low resolution camera, cloud texture can be distinguished.

(a) Lepton mounted on Raspberry Pi for data collection.

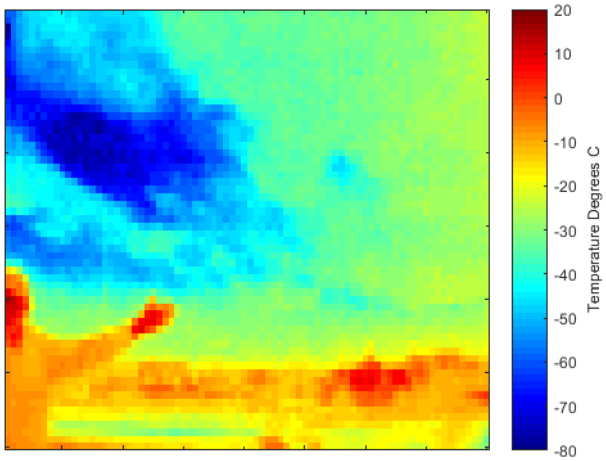

(b) Lepton image shows a human figure waving, with clouds and campus buildings in the background.

Figure 4: Lepton data collection and demonstration.

To confirm the camera was operating as expected for measurement purposes, a human hand was placed in front of a calibrated blackbody at two different temperatures for contrast. Figure 5a shows a hand in front of a 20 °C blackbody, and Fig. 5b shows a hand in front of a 60 °C blackbody. Since human skin is very emissive, it is expected to be approximately 32 °C in brightness temperature.

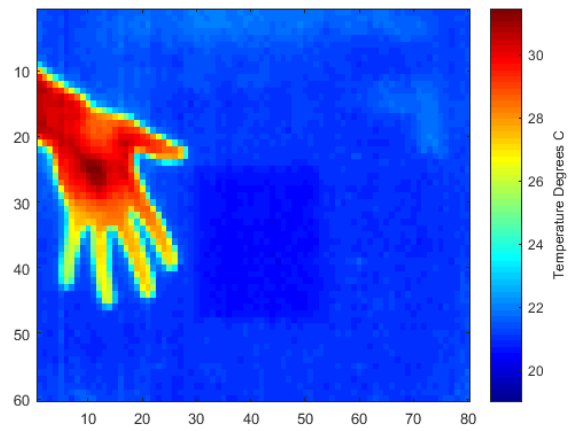

(a) Calibrated Lepton image showing a 20 °C blackbody.

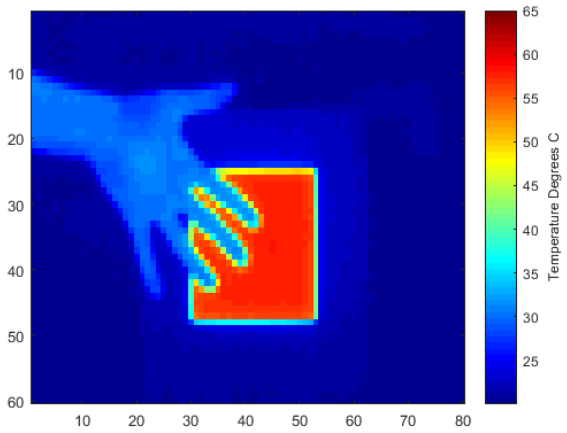

(b) Calibrated Lepton image showing a 60 °C blackbody.

Figure 5: Lepton calibration visual validation.

4. LEPTON CALIBRATION LIMITATIONS

We calibrated the mechanical shutter version of the Lepton when the camera first came out in the summer of 2016. As these data were analyzed, the Lepton camera showed a distinct exponential rise and decay in digital number as a response to the time of the last flat field correction, as shown in Fig. 6. It seemed like the FPA was receiving an internal impulse heat signature, and was slowly heating and cooling in response. This led to the theory that the internal shutter mechanism was being driven by a solenoid that would quickly dump current as the attached shutter was moved into position for the flat field correction. This current would be dumped into a resistor, which heated up in response. This heat was significant enough in relative terms to the thermal mass of the FPA to have a large contribution on FPA temperature. Because of this, it would follow that the behavior could be predicted and compensated for through camera characterization.

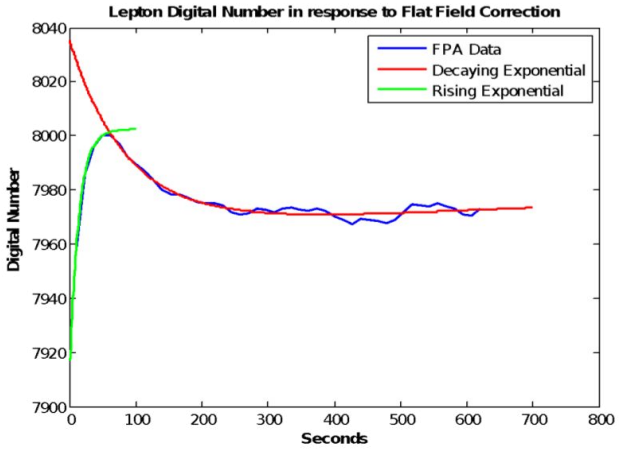

Figure 6: Camera FPA temperature compensation requires an exponential time component due to mechanical shutter.

The exponential thermal detector response with respect to FFC time was found through statistical analysis of the a second-order exponential curve fit of detector responses over time for a random subset of 7,500 images. The decaying second-order exponential was then applied to the calibration as part of a robust matrix inversion

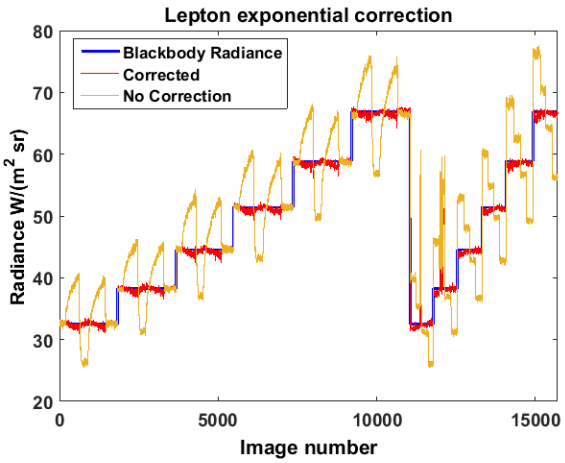

(a) Known blackbody radiance compared to corrected average image radiance.

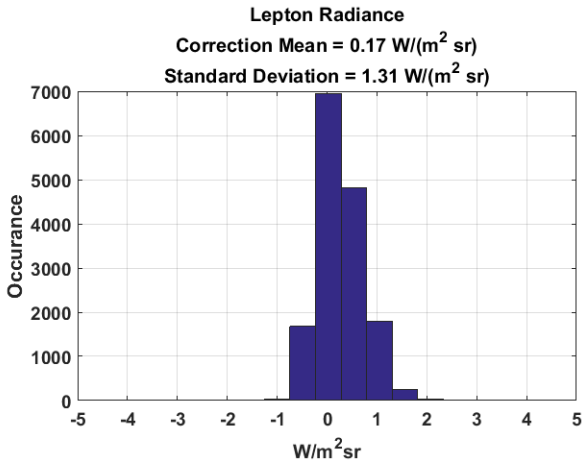

(b) Distribution of error between blackbody and corrected radiance

Figure 7: Lepton calibration using linear regression.

to back out the radiometric calibration. The results of the calibrated average radiance with respect to actual blackbody radiance is shown in Fig. 7. Using this method, the standard deviation of radiometric error is 1.31 W/(m^2 sr), in comparison to 1.57 W/(m^2 sr) from our previous calibration. This method shows promise, and should be further investigated if this particular camera is to be used for high-accuracy field experiments.

In the data set there existed an error during the second blackbody ramp from data points 11300 to 11400 and from 11900 to 12200. The cause of these errors is unknown, but the two likely candidates are synchronization errors in the SPI data frame acquisition interface or an improper flat field correction. If these data are excluded from the analysis, standard deviation for the Lepton camera with the standard MSU calibration reduced to 0.89 W/(m^2 sr), and for the exponential correction it reduced to 0.44 W/(m^2 sr).

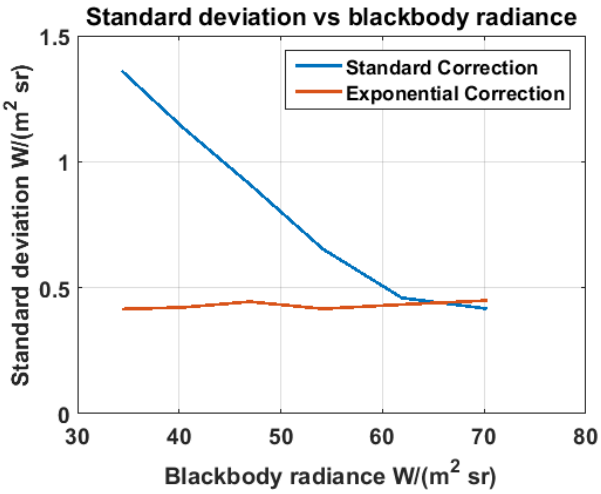

Figure 8: Lepton calibration error for the exponential correction is fairly flat with respect to blackbody radiance.

In Fig. 8 the standard deviation of the error between blackbody radiance and calibrated radiance at each blackbody temperature is shown. The exponential-based correction performs equally well at all blackbody scenes, whereas the Lepton imager with the standard MSU correction has decreasing performance as the blackbody radiance (scene temperature) decreases.

5. CONCLUSION

The Lepton was able to be radiometrically calibrated with a high level of repeatability for blackbody targets. A RMS value of 1.57 W/(m^2 sr) was achieved for the Lepton correction using standard microbolometer calibration methods. Using an exponential-based algorithm that accounted for temperature compensation vs time, a 1.31 W/(m^2 sr) RMS error was achieved. This shows that even ultra-low-cost IR imaging modules can be calibrated to perform quantitative radiometric measurements.

Disclosures

The authors have no relevant financial interests in the manuscript and no other potential conflicts of interest to disclose.

ACKNOWLEDGMENTS

The authors gratefully acknowledge funding from the Montana Research and Economic Development Initiative (MREDI), through award 51040-MUSRI2015-01.

REFERENCES

[1] Shaw, J. A., Nugent, P. W., Johnson, J., Bromenshenk, J. J., Henderson, C. B., and Debnam, S., "Long-wave infrared imaging for non-invasive beehive population assessment," *Opt. Express* **19**, 399–408 (Jan 2011).

[2] Nugent, P. W., Shaw, J. A., and Vollmer, M., "Colors of thermal pools at Yellowstone National Park," *Appl. Opt.* **54**, B128–B139 (Feb 2015).

[3] Shaw, J. A., Nugent, P. W., Harris, W., and Vollmer, M., "Infrared Yellowstone," *Opt. Photon. News* **28**(6), 36–43 (2017).

[4] Johnson, J. E., Shaw, J. A., Lawrence, R., Nugent, P. W., Dobeck, L. M., and Spangler, L. H., "Long-wave infrared imaging of vegetation for detecting leaking CO2 gas," *Journal of Applied Remote Sensing* **6**(1), 063612–063612 (2012).

[5] Shaw, J. A., Nugent, P. W., Pust, N. J., Thurairajah, B., and Mizutani, K., "Radiometric cloud imaging with an uncooled microbolometer thermal infrared camera," *Opt. Express* **13**, 5807–5817 (Jul 2005).

[6] Thurairajah, B. and Shaw, J. A., "Cloud statistics measured with the infrared cloud imager (ICI)," *IEEE Transactions on Geoscience and Remote Sensing* **43**(9), 2000–2007 (2005).

[7] Shaw, J. A. and Nugent, P. W., "Physics principles in radiometric infrared imaging of clouds in the atmosphere," *European Journal of Physics* **34**(6), S111 (2013).

[8] Nugent, P. W., *Deployment of the third-generation infrared cloud imager, a two year study of arctic clouds at Barrow Alaska*, PhD thesis, Montana State University (4 2016).

[9] Nugent, P. W., Shaw, J. A., and Piazzolla, S., "Infrared cloud imaging in support of earth-space optical communication," *Opt. Express* **17**, 7862–7872 (May 2009).

[10] Shaw, J. A., Nugent, P. W., Pust, N. J., Redman, B. J., and Piazzolla, S., "Cloud optical depth measured with ground-based uncooled infrared imagers," in [*Proc. SPIE*], **8523**, 85231D (2012).

[11] Nugent, P. W., Shaw, J. A., and Piazzolla, S., "Infrared cloud imager development for atmospheric optical communication characterization, and measurements at the JPL Table Mountain Facility," *Interplanetary Network Progress Report* (42–192), 1–30 (2013).

[12] Riesland, D. W., Nugent, P. W., Shaw, J. A., Zemba, M. J., and Houts, J., "Infrared cloud imaging in support of Ka-Band progagation studies," in [*AIAA Proc. International Communications Satellite Systems Conference*], (2016).

[13] Shaw, J. A., Nugent, P. W., and Vollmer, M., "Infrared moon imaging for remote sensing of atmospheric smoke layers," *Appl. Opt.* **54**, B64–B75 (Feb 2015).

[14] Nugent, P. W., Shaw, J. A., and Pust, N. J., "Correcting for focal-plane-array temperature dependence in microbolometer infrared cameras lacking thermal stabilization," *Optical Engineering* **52**(6), 061304–061304 (2013).

[15] Nugent, P. W. and Shaw, J. A., "Calibration of uncooled LWIR microbolometer imagers to enable long-term field deployment," in [*SPIE Defense+ Security*], 90710V–90710V, International Society for Optics and Photonics (2014).

[16] Nugent, P. W., Shaw, J. A., and Pust, N. J., "Radiometric calibration of infrared imagers using an internal shutter as an equivalent external blackbody," *Optical Engineering* **53**(12), 123106–123106 (2014).